Wave modes in shear-deformed two-dimensional plasma crystals

A. V. Ivlev,[1,*] T. B. Röcker,[1] L. Couëdel,[2] V. Nosenko,[3] and C.-R. Du[4]
[1]*Max-Planck-Institut für Extraterrestrische Physik, 85741 Garching, Germany*
[2]*CNRS, Aix Marseille Université, Laboratoire PIIM, 13397 Marseille Cedex 20, France*
[3]*Forschungsgruppe Komplexe Plasmen, Deutsches Zentrum für Luft- und Raumfahrt, 82234 Weßling, Germany*
[4]*College of Science, Donghua University, Shanghai 201620, People's Republic of China*
(Received 9 March 2015; published 25 June 2015)

A theory of wave modes in shear-deformed two-dimensional plasma crystals is presented. Modification of the dispersion relations upon the pure and simple shear, and the resulting effect on the onset of the mode-coupling instability, are studied. In particular, it is explained why the velocity fluctuation spectra measured in experiments with sheared crystals exhibit asymmetric "hot spots": It is shown that the coupling of the in-plane compressional and the out-of-plane modes, leading to the formation of an unstable hybrid mode and generation of the hot spots, is enhanced in a certain direction determined by deformation.

DOI: 10.1103/PhysRevE.91.063108 PACS number(s): 52.27.Lw, 52.27.Gr, 52.35.−g

I. INTRODUCTION

Experimental particle-resolved studies of generic strong-coupling phenomena are carried out using natural model systems, such as complex plasmas and colloidal dispersions [1,2]. Two-dimensional (2D) model systems enable us to observe the individual particle dynamics of the entire ensemble in the greatest detail, both in space and time. In particular, recent experiments with 2D complex plasmas made it possible to perform particle-resolved studies of equilibrium and nonequilibrium melting [3,4], diffusion [5,6], onset of plastic deformations [7], dynamics of dislocations [8], etc. Such systems are usually obtained in radiofrequency (rf) plasma discharge chambers [9–12], where the negatively charged microparticles levitate above a flat horizontal rf electrode due to the balance between gravity and electrostatic forces. By tuning the experimental conditions, one can obtain a crystalline monolayer, the so-called 2D plasma crystal, where microparticles form a hexagonal lattice.

The use of complex plasmas as a model system requires that certain plasma-specific phenomena, associated with the energy and momentum exchange between charged microparticles and ions or electrons of the surrounding discharge, play only a minor role. For 2D complex plasmas, the most notable phenomena include charge-fluctuation instabilities (associated with the fact that the charge of a microparticle fluctuates around the equilibrium value, which, in turn, varies in space) [13–16], and mode-coupling instability (MCI) [17–21]. The effect of charge fluctuations, leading to single-particle instabilities, is easily made negligible by a slight increase of gas pressure (i.e., of frictional damping for particles) [15,16]. On the contrary, the MCI is the collective nonequilibrium phenomenon, which turns out to be the prime cause of the plasma-specific melting of 2D crystals [21].

The MCI is associated with the wake-mediated interactions between microparticles levitating in the sheath above the electrode: In the presence of a strong vertical plasma flow driven by the sheath field, the screening cloud around each charged particle becomes highly perturbed and asymmetric [22–25]. These clouds are usually referred to as "plasma wakes" [26–31]. The wakes exert attractive forces on the neighboring particles and make the pair interactions nonreciprocal [32–34]. The MCI is triggered by a resonant coupling of the in-plane compressional (acoustic) and out-of-plane (optical) wave modes, due to the nonreciprocal particle-wake interactions [17,18,20]. The MCI has a well-defined confinement-density threshold (determined by a combination of the vertical confinement strength and the particle number density in the monolayer), above which the wave modes do not cross and, therefore, the MCI is completely disabled [21,35].

Even in the most accurate experiments, 2D plasma crystals never have a perfect crystalline order. One of the main reasons for that is the presence of a weak horizontal confinement (presumably exerted due to edge effects in the discharge) [36–40]. Often, this confinement has azimuthal asymmetry [41,42], which inevitably creates a weak shear strain in a crystal. Even though such weak deformations may have only a minor impact on some generic processes studied with 2D complex plasmas, for the critical phenomena (in particular, for the onset of the MCI) the effect can be profound. Recent experiments [43] indicate that the development of the MCI in a slightly sheared crystal becomes highly asymmetric.

In this paper, we present a theory of wave modes in shear-deformed 2D plasma crystals. We study the effects of pure and simple shear on the dispersion relations and on the onset of the MCI. In particular, we explain the effect of asymmetric hot spots seen in experimentally measured velocity fluctuation spectra of sheared crystals: It is shown that resonant mode coupling, which leads to the formation of an unstable hybrid mode and generates the hot spots, is modified in a deformed crystal. The wave modes participating in the coupling become deformed in such a way that their crossing first occurs in a certain direction determined by the applied shear.

II. DYNAMICAL MATRIX FOR A DEFORMED LATTICE

A homogeneous compression of a 2D plasma crystal does not change the wave modes themselves—it only leads to a trivial rescaling of the frequency ω and wave vector $\mathbf{k}$, and it changes the value of the MCI threshold [21,35]. In typical experiments with 2D plasma crystals [4,8,19,35], the

*ivlev@mpe.mpg.de

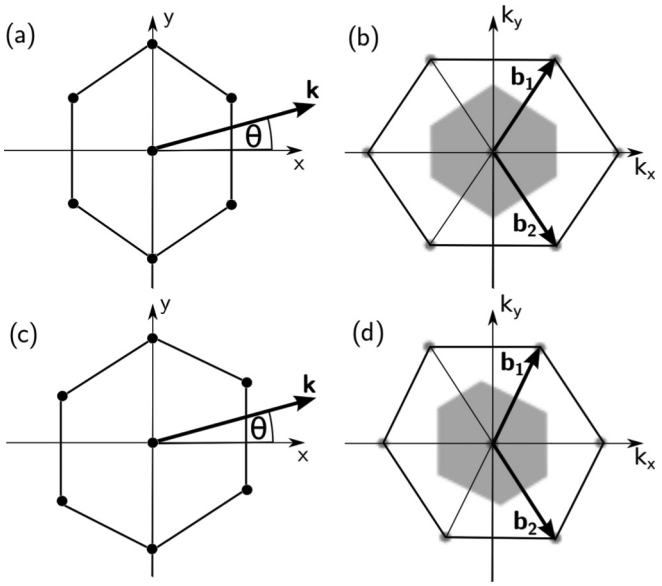

FIG. 1. Sheared hexagonal lattice cells (left) and the corresponding reciprocal-lattice cells in **k** space (right). The upper row (a,b) and lower row (c,d) show the cases of pure and simple shear, respectively. Upon pure shear, the crystalline lattice is contracted (by the factor $\mu = 0.924$) along the x axis (a), so for the reciprocal lattice the contraction is in the k_y direction (b). Upon simple shear, the strain (of $\tau = 0.08$) is in the y direction (c), so in the reciprocal space the strain is along the k_x axis (d). The basis vectors $\mathbf{b}_{1,2}$ of the reciprocal lattice are shown; the gray regions within the reciprocal cells are the first Brillouin zones.

interparticle distance is practically constant in the center of the monolayer. Therefore, here we shall assume the particle density (and hence the particle charge) to be constant as well, and we focus on shear deformations that can be generally decomposed into the pure and simple shear [44], as shown in Fig. 1.

We note that the dispersion relation $\omega(\mathbf{k})$ of wave modes in a shear-deformed 2D plasma crystal can be straightforwardly derived from the dynamical matrix $\mathbf{D}(\mathbf{k})$ for a perfect (regular) hexagonal lattice (see Appendix): The dispersion and coupling elements of $\mathbf{D}(\mathbf{k})$, Eqs. (A2) and (A3), are determined by the normalized lattice vectors $\mathbf{s}^*$ (measured in units of the interparticle distance Δ). These vectors characterize the equilibrium positions of particles in a regular lattice, so for our problem they have to be replaced with the vectors $\mathbf{s}$ of a deformed lattice.

In a general case, the shear transformation of the lattice vectors has the following form:

$$\mathbf{s} = \mathbf{T}\mathbf{R}\,\mathbf{s}^*, \tag{1}$$

where $\mathbf{R}$ is the rotation matrix in the lattice plane, which depends on the angle between the applied shear and (one of) the principal axes of the regular lattice, and $\mathbf{T}$ is the deformation matrix due to the shear. Let us characterize the pure (p) shear by the contraction (or extension) factor μ, and the simple (s) shear by the strain τ. The corresponding lattice deformations are illustrated in Figs. 1(a) and 1(c). In both cases, the shear is applied along the principal lattice axes, so $\mathbf{R}$ is the unity matrix and the respective deformation matrices have the following form:

$$\mathbf{T}_\mathrm{p} = \begin{pmatrix} \mu & 0 \\ 0 & \mu^{-1} \end{pmatrix}, \qquad \mathbf{T}_\mathrm{s} = \begin{pmatrix} 1 & 0 \\ \tau & 1 \end{pmatrix}. \tag{2}$$

For pure shear, we say the lattice is contracted (extended) when $\mu < 1$ (>1). Obviously, the contraction μ in one direction is equivalent to the extension $1/\mu$ in the perpendicular direction; for simple shear, the effects of positive and negative strains (of the same magnitude) are equivalent upon the switch $\theta \to -\theta$. Note that a combination of pure and simple shear with given μ and τ is not commutative, since $\mathbf{T}_\mathrm{p}\mathbf{T}_\mathrm{s} \neq \mathbf{T}_\mathrm{s}\mathbf{T}_\mathrm{p}$.

The resulting deformations of the reciprocal lattice in **k** space are shown in Figs. 1(b) and 1(d). The reciprocal deformation matrix is the inverse transpose of $\mathbf{T}$. Therefore, the basis vectors $\mathbf{b}_{1,2}$ of a deformed reciprocal lattice are related to the basis $\mathbf{b}^*_{1,2} = 2\pi\Delta^{-1}(\frac{1}{\sqrt{3}}, \pm 1)$ of the regular lattice via $\mathbf{b}_{1,2} = (\mathbf{T}^{-1})^T\mathbf{b}^*_{1,2}$.

The area of the first Brillouin zone naturally remains unchanged by shear. Note, however, that the hexagonal zones in real and reciprocal space are not similar: For instance, while the x-to-y aspect ratio of the hexagon in real space varies upon pure shear as $\propto \mu^2$, the respective (k_y-to-k_x) ratio scaling in reciprocal space is $\propto \mu^2 + 1/(3\mu^2)$.

III. EXPERIMENTAL EXAMPLE

In the experiment shown in Fig. 3 of Ref. [43], the deformation was apparently caused by a combination of the pure and simple shear. In Fig. 2 we present another experiment, performed under similar discharge conditions (gas pressure 0.9 Pa, forward rf power 20 W, and microparticle diameter 9.19 μm). We were able to create the pure shear deformation with practically no contribution of the simple shear. Moreover, in this case the crystal was contracted along the principal lattice direction, corresponding to the x axis in Fig. 1. The contraction factor was $\mu = 0.924$, as one can

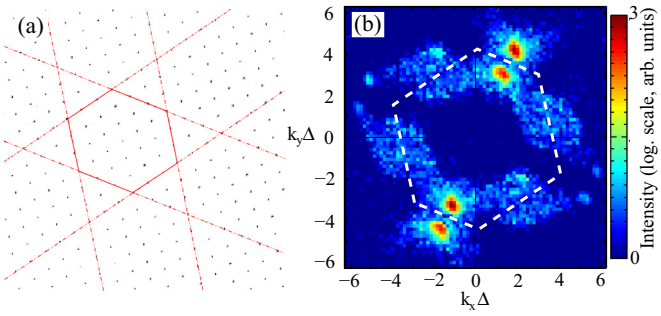

FIG. 2. (Color online) Example of a sheared 2D plasma crystal observed in experiments. (a) The hexagonal lattice is subject to pure shear, resulting in the contraction with $\mu = 0.924$ along one of the principal lattice axes [as in Fig. 1(a)]. The thin solid lines drawn along the lattice axes are a guide for the eye. (b) The velocity fluctuation spectrum integrated over frequency (in the range $18.5 < f < 21.5$ Hz) demonstrates the asymmetric mode coupling—generation of the hot spots in the direction of contraction (instead of the regular patterns with a period of 60°). The hot spots emerge near the border of the first Brillouin zone, obtained from the lattice structure factor (indicated by the dashed line).

directly deduce from Fig. 2(a). The corresponding frequency-integrated fluctuation spectrum, i.e., the intensity distribution of the velocity fluctuations in the **k** plane, is plotted in Fig. 2(b). We see that the "hot spots," which are a signature of the unstable hybrid mode [19,21,35], were generated for **k** parallel to the direction of contraction. This is a clear manifestation of the asymmetry introduced by the shear in the wake-induced mode coupling.

To explain the observed behavior and understand general principles governing modification of the wave modes upon shear, let us separately consider the dispersion relations in a crystal subject to pure and simple shear.

IV. MODIFICATION OF THE WAVE MODES

The dispersion relations $\omega(\mathbf{k})$ are obtained in a usual way from Eq. (A4) using the dynamical matrix for shear-deformed lattices. For the calculations below, we use the point-wake interparticle interaction, Eq. (A5). The interactions are characterized by the screening parameter $\kappa = \Delta/\lambda$, and the wake parameters are expressed in terms of the dimensionless wake charge $\tilde{q} = q/Q$ and length $\tilde{\delta} = \delta/\Delta$. The wave vector is normalized by the inverse of the lattice constant Δ, while the frequency is in units of the effective dust-lattice (DL) frequency scale Ω_{DL} [17,18], i.e., $\mathbf{k}\Delta \to \mathbf{k}$ and $\omega/\Omega_{\mathrm{DL}} \to \omega$. We define Ω_{DL} as [21,35]

$$\Omega_{\mathrm{DL}} = \sqrt{\frac{(1-\tilde{q})Q^2}{M\lambda^3}}.$$

Since the particle charge Q is expected to depend primarily on the mean density in the monolayer (e.g., Ref. [15]), here we assume that Q is not affected by shear deformation.

To illustrate the theoretical results, we chose the following dimensionless parameters: $\kappa = 1$, $\tilde{q} = 0.4$, and $\tilde{\delta} = 0.37$, representing typical MCI experiments [21,45]. Different regimes of the mode coupling are demonstrated by varying the (normalized) confinement frequency, i.e., the value of $\omega(0) = \Omega_{\mathrm{conf}}$ for the optical out-of-plane mode. For simplicity, we show the undamped dispersion relations [35].

A. Pure shear

Figure 3 illustrates how the wave modes in a hexagonal lattice are modified by the pure shear. The upper panel shows how the theoretical dispersion relations change upon the contraction by the factor $\mu = 0.924$, corresponding to the experiment in Fig. 2. As expected, the strongest effect is on the in-plane shear (transverse) mode, whose frequency is substantially increased for the waves propagating along the two principal lattice axes. Another important effect is on the relative shift of the in-plane compressional (longitudinal) and the out-of-plane branches: We see that in the direction of contraction ($\theta = 0^\circ$), the branches slightly approach each other near the border of the first Brillouin zone (primarily, due to decrease of the out-of-plane wave frequency), whereas in the perpendicular direction ($\theta = 90^\circ$) the branches become more separated (due to a substantial decrease of the compressional wave frequency). The effect of extension by the factor $\mu = 1/0.924 = 1.08$, shown in the lower panel, is also intuitive—it is basically opposite to that of the contraction.

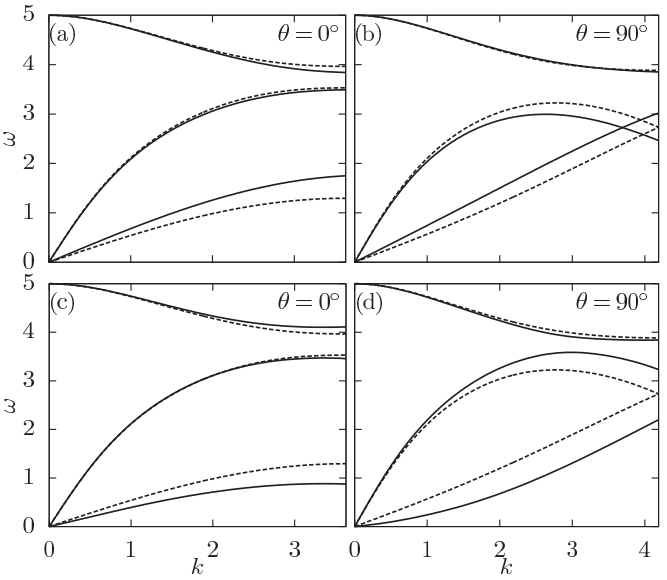

FIG. 3. Modification of the wave modes in a hexagonal lattice under pure shear. The upper row (a,b) is for the contraction with $\mu = 0.924$ (corresponding to the experiment in Fig. 2), while the lower row (c,d) demonstrates the effect of extension with $\mu = 1/0.924 = 1.08$. The solid lines show the dispersion relations in the sheared crystal, and the dashed lines are for the regular (unsheared) hexagonal lattice. The upper and lower acoustic branches are the in-plane compressional and shear modes, respectively, and the optical branch is the out-of-plane mode. The left and right panels depict the dispersion relations for $\theta = 0^\circ$ and 90°, respectively [see Fig. 1(a)].

The influence of pure shear on the wake-induced mode coupling is presented in Fig. 4. Here, the confinement frequency is set slightly lower than in the previous figure, so the in-plane compressional and the out-of-plane modes may intersect near the border of the first Brillouin zone, and thus the asymmetry introduced in the mode coupling can be revealed.

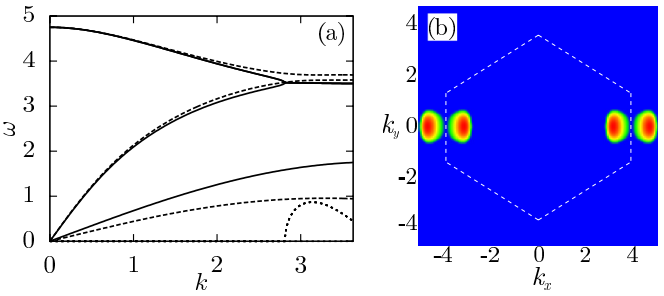

FIG. 4. (Color online) Onset of the asymmetric wake-induced mode coupling under pure shear ($\mu = 0.924$). (a) The dispersion relations for $\theta = 0^\circ$ (solid lines) and $\theta = 60^\circ$ (dashed lines) are different due to the shear-induced asymmetry. Therefore, the in-plane compressional (acoustic) and out-of-plane (optical) modes first intersect in the direction of contraction, forming an unstable hybrid mode with a nonzero imaginary part [the dotted line shows the growth rate $\mathrm{Im}\omega(k)$ multiplied by 10]. (b) The contour plot of the growth rate for the hybrid mode, emerging near the border of the first Brillouin zone (indicated by the dashed line) and representing the hot spots observed in the experiment [Fig. 2(b)].

In a regular hexagonal lattice, the branches for $\theta = 0^\circ$ and 60° are identical, but in a sheared lattice this symmetry is broken and the modes approach closer to each other in the direction of contraction. Therefore, in Fig. 4(a) we observe the unstable hybrid mode formed for $\theta = 0^\circ$, while for $\theta = 60^\circ$ the branches are still separated. The contour plot of the MCI growth rate $\mathrm{Im}\omega(\mathbf{k})$, shown in Fig. 4(b), provides an excellent representation of the hot spots seen in experimental fluctuation spectra [Fig. 2(b)].

The applied shear does not introduce any qualitative changes in a coupling between the in-plane shear and the out-of-plane modes: From the general dispersion relation, Eqs. (A1) and (A4), we derive the condition of exact *decoupling* of the shear mode,

$$\beta\sigma_x\sigma_y + \gamma\left(\sigma_x^2 - \sigma_y^2\right) = 0. \tag{3}$$

Analysis of Eq. (3) shows that for a regular hexagonal lattice, it is satisfied identically along the principal axes: Due to the lattice symmetry, the dispersion element γ and one of coupling elements, σ_x or σ_y, are equal to zero for $\theta = n \times 30^\circ$ (where n is an integer). Upon pure shear, the lattice symmetry is still preserved along the directions $\theta = 0^\circ$ and 90°, where the modified shear mode remains decoupled; for intermediate directions, the resulting hybrid mode is only slightly affected by such deformation.

Finally, we discuss the anisotropy of the wave modes, which is introduced by the pure shear. For a regular hexagonal lattice, the long-wavelength dispersion relations of all three modes are known to be independent on the direction of $\mathbf{k}$ [44]; they have the form $\omega_{\mathrm{o}}^2(\mathbf{k})|_{k\to 0} = \Omega_{\mathrm{conf}}^2 - C_{\mathrm{o}}^2 k^2$ for the out-of-plane mode and $\omega_{\mathrm{s,c}}^2(\mathbf{k})|_{k\to 0} = C_{\mathrm{s,c}}^2 k^2$ for the in-plane modes (where $C_{\mathrm{s,c}}^2$ are the squared acoustic velocities of the shear and compressional waves) [46–49]. In a deformed lattice, the factors C^2 (below we term them "squared velocities" for all three modes) naturally become periodic functions of θ with a period of 180°, as shown in Figs. 5(a)–5(c). Due to the shear symmetry, these are even functions whose extrema are attained when $\mathbf{k}$ is parallel to one of the principal axes. As expected, the lattice contraction (μ) and extension ($1/\mu$) lead to the opposite effects, but the resulting magnitudes are noticeably different. To quantify the amplitude of the anisotropy, in Fig. 5(d) we plot the parameter ΔC^2 versus the shear factor μ, defined for each mode as the difference $C^2(\mu) - C^2(1)$ measured at $\theta = 0^\circ$. We see that even for very small deformations, the anisotropy of the squared velocities (in particular, of C_{c}^2) exhibits a significant nonlinear (quadratic) dependence on μ.

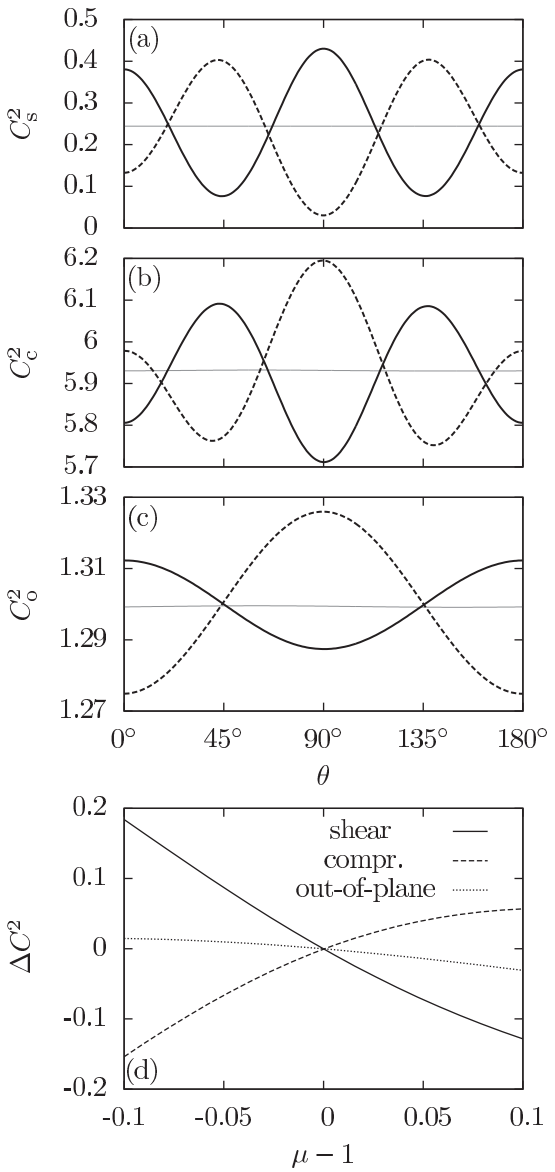

FIG. 5. Anisotropy of the long-wavelength wave modes upon the pure shear. Shown are the squared velocities C^2, determining the dispersion relations of the acoustic shear (a) and compressional (b) wave modes as well as of the optical out-of-plane mode (c) in the limit $k \to 0$, plotted vs the angle θ. The solid and dashed lines illustrate the contraction ($\mu = 0.924$) and extension ($\mu = 1/0.924 = 1.08$), respectively, and the thin horizontal lines are for a regular lattice ($\mu = 1$). The lower panel (d) presents the dependence of the anisotropy amplitude ΔC^2 on μ.

B. Simple shear

All qualitative effects occurring with the wave modes upon pure shear and discussed in the previous section are also observed when simple shear is applied. The only difference is that now the extrema of the squared velocities are located at certain intermediate angles, $\neq 0^\circ$ or 90°, determined (for each mode) by the magnitude of strain τ. Since the x and y axes are no longer the axes of symmetry, the shear mode is coupled to the out-of-plane mode also in these directions.

Figure 6 illustrates the coupling between the in-plane shear and the out-of-plane modes along the x and y axes. The confinement frequency is further lowered (as compared to Fig. 4) to allow the mode crossing and demonstrate that the "shear" hybrid mode (in addition to the usual—"compressional"—hybrid mode) is also formed in these directions. Apart from this, the dispersion relations for the simple shear exhibit exactly the same qualitative features as those presented for the pure shear in Figs. 3 and 4.

In Figs. 7(a)–7(c) we present the squared velocities of the three modes as functions of θ. For symmetry reasons, $C^2(\theta)$ for a positive strain is equal to $C^2(180^\circ - \theta)$ for a negative strain of the same magnitude. The dependence of the anisotropy

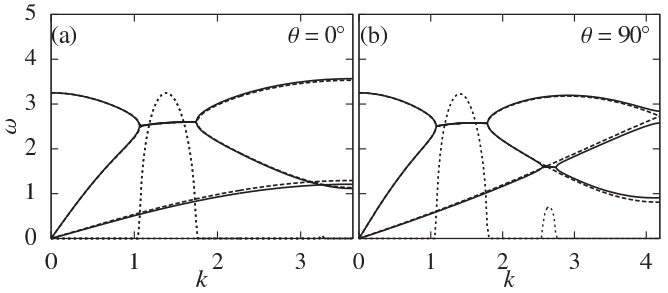

FIG. 6. Wake-induced coupling of the in-plane shear mode, modified by simple shear with the strain $\tau = 0.08$. The branches for $\theta = 0^\circ$ (a) and $\theta = 90^\circ$ (b) are plotted; the solid lines show the dispersion relations in the sheared crystal, and the dashed lines are for the regular (unsheared) lattice. The out-of-plane (optical) mode crosses both the compressional (upper acoustic) and shear (lower acoustic) modes, and the dotted lines show the imaginary part of the resulting hybrid modes, $\mathrm{Im}\omega(k)$, multiplied by 10.

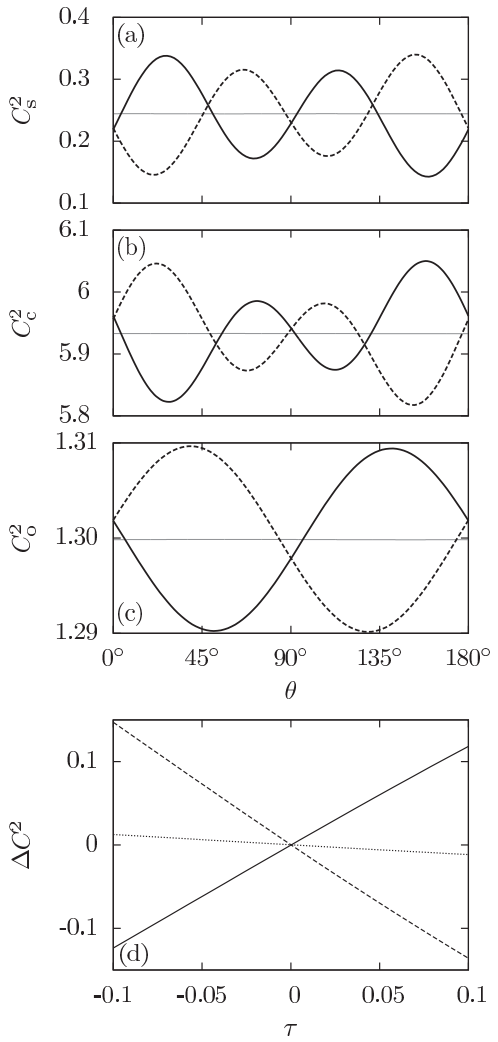

FIG. 7. Same as in Fig. 5, plotted for the simple shear vs the strain τ. The solid and dashed lines in (a)–(c) illustrate the positive ($\tau = 0.08$) and negative ($\tau = -0.08$) strain, respectively.

amplitude ΔC^2 on the strain τ is plotted in Fig. 7(d); for simple shear, we define ΔC^2 as the difference $C^2(\tau) - C^2(1)$ measured at the first extremum. Unlike the pure shear case, now the anisotropy scales linearly with τ for deformations of up to ∼10% (a weak quadratic correction is observed for C_c^2).

V. CONCLUSIONS

We presented the basic characterization of the wave modes in shear-deformed 2D plasma crystals. The dynamical matrix for a crystal under pure or simple shear can be directly obtained from the matrix for a regular hexagonal lattice by performing a shear transformation of the lattice vectors.

We showed that, both for simple and pure shear, the wave modes exhibit qualitatively similar features: The dispersion relations become asymmetric, i.e., the dependence $\omega(\mathbf{k})$ has a period of 180° (instead of the 60° periodicity for the regular lattice). Most notably, this asymmetry is revealed in the asymmetric mode coupling, when the in-plane compressional and the out-of-plane modes form an unstable hybrid mode in a certain direction determined by deformation (e.g., along the contraction upon the pure shear). This finding explains the generation of asymmetric hot spots observed in experimental fluctuation spectra for sheared crystals.

We expect that detailed verification of our theoretical findings related to the critical modification of the wave modes upon the shear (such as the mode-coupling asymmetry) can be carried out in dedicated experiments with deformed plasma crystals.

ACKNOWLEDGMENTS

The authors acknowledge support from the European Research Council under the European Union's Seventh Framework Programme, Grant Agreement No. 267499.

APPENDIX: GENERAL FORM OF THE DYNAMICAL MATRIX

Linear dispersion relations $\omega(\mathbf{k})$ of wave modes in a crystal are determined by eigenvalues of a dynamical matrix $\mathbf{D}(\mathbf{k})$. The latter is derived by considering small perturbations of individual particles (with respect to a stable crystalline configuration) of the form $\propto e^{-i\omega t + i\mathbf{k}\cdot\mathbf{r}}$. Elements of $\mathbf{D}(\mathbf{k})$ are given by the lattice sums determined by the particle potential $\phi(\mathbf{r})$. If the interactions are reciprocal, then $\mathbf{D}$ is Hermitian, the eigenvalues in this case are real (i.e., the modes are stable), and the eigenvectors are orthogonal. For nonreciprocal interactions, i.e., when $\partial\phi(\mathbf{r}_{ij})/\partial\mathbf{r}_i \neq -\partial\phi(\mathbf{r}_{ij})/\partial\mathbf{r}_j$ for a pair of particles i and j, the eigenvalues can be complex (so the modes become unstable) [18,21,35].

For nonreciprocal interparticle interactions in 2D plasma crystals, the dynamical matrix has the following form [18,21,35]:

$$\mathbf{D} = \begin{pmatrix} \alpha_h - \beta & 2\gamma & i\sigma_x \\ 2\gamma & \alpha_h + \beta & i\sigma_y \\ i\sigma_x & i\sigma_y & \Omega_{\mathrm{conf}}^2 - 2\alpha_v \end{pmatrix}. \quad \text{(A1)}$$

The matrix is calculated for the reference frame shown in Fig. 1, assuming that the particles are confined to the plane

$z = 0$ in a parabolic potential well with the eigenfrequency Ω_{conf}. The dispersion elements $\alpha_{\text{h,v}}(\mathbf{k})$, $\beta(\mathbf{k})$, and $\gamma(\mathbf{k})$ are given by the sums over integer m and n with excluded (0,0),

$$\alpha_{\text{h}},\beta = \frac{Q}{M}\sum_{m,n}\left(\frac{\partial^2\phi}{\partial y^2} \pm \frac{\partial^2\phi}{\partial x^2}\right)\Bigg|_{\mathbf{r}=\mathbf{s}} \sin^2\frac{1}{2}\mathbf{k}\cdot\mathbf{s},$$
$$\gamma = \frac{Q}{M}\sum_{m,n}\frac{\partial^2\phi}{\partial x\partial y}\Bigg|_{\mathbf{r}=\mathbf{s}} \sin^2\frac{1}{2}\mathbf{k}\cdot\mathbf{s}, \tag{A2}$$
$$\alpha_{\text{v}} = -\frac{Q}{M}\sum_{m,n}\frac{\partial^2\phi}{\partial z^2}\Bigg|_{\mathbf{r}=\mathbf{s}} \sin^2\frac{1}{2}\mathbf{k}\cdot\mathbf{s},$$

and the coupling elements $\sigma_{x,y}(\mathbf{k})$ are

$$\sigma_{x,y} = -\frac{Q}{M}\sum_{m,n}\frac{\partial^2\phi}{\partial\{x,y\}\partial z}\Bigg|_{\mathbf{r}=\mathbf{s}} \sin\mathbf{k}\cdot\mathbf{s}, \tag{A3}$$

where Q and M are the particle charge and mass, respectively. The normalized 2D lattice vectors $\mathbf{s}(m,n)$ (measured in units of the interparticle distance Δ) identify the equilibrium positions of neighboring particles in a crystal. In a regular hexagonal lattice, $\mathbf{s} = \mathbf{s}^*$ with the components $s_x^* = \frac{\sqrt{3}}{2}m$ and $s_y^* = \frac{1}{2}m + n$.

The dispersion relations $\omega(\mathbf{k})$ are obtained from the following equation:

$$\det[\mathbf{D} - \omega(\omega + i\nu)\mathbf{I}] = 0, \tag{A4}$$

where $\mathbf{I}$ is the unit matrix and ν is the damping rate entering the particle equation of motion. Thus, $\omega(\omega + i\nu)$ is the eigenvalue of the dynamical matrix.

Theoretical investigations of the MCI are often based on a simple "Yukawa/point-wake model" [17,18,35], where the wake is considered as a (positive) pointlike effective charge q located at the distance δ below each (negatively charged) particle. Thus, the total interaction between two particles is a simple superposition of the particle-particle and particle-wake interactions, both described by the (spherically symmetric) Yukawa potentials with the effective screening length λ,

$$\phi(\mathbf{r}) = -\frac{Q}{r}e^{-r/\lambda} + \frac{q}{r_\delta}e^{-r_\delta/\lambda}, \tag{A5}$$

where $r = |\mathbf{r}|$ and $r_\delta = |\mathbf{r} + \delta\mathbf{n}_z|$. The elements of the dynamical matrix for such interactions have been calculated for "weak" [18,35] and "strong" [21,50] wakes, determined by the relative magnitude of the wake dipole $q\delta$. Recently, it was shown that more sophisticated kinetic models can provide a better description of the dispersion relations, in particular for the out-of-plane mode [45,51].

[1] A. Ivlev, H. Löwen, G. Morfill, and C. P. Royall, *Complex Plasmas and Colloidal Dispersions: Particle-Resolved Studies of Classical Liquids and Solids* (World Scientific, Singapore, 2012).

[2] M. Bonitz, C. Henning, and D. Block, Rep. Prog. Phys. **73**, 066501 (2010).

[3] C. L. Chan, W. Y. Woon, and L. I, Phys. Rev. Lett. **93**, 220602 (2004).

[4] V. Nosenko, S. K. Zhdanov, A. V. Ivlev, C. A. Knapek, and G. E. Morfill, Phys. Rev. Lett. **103**, 015001 (2009).

[5] Y. J. Lai and L. I, Phys. Rev. Lett. **89**, 155002 (2002).

[6] T. Ott and M. Bonitz, Phys. Rev. Lett. **103**, 195001 (2009).

[7] V. Nosenko, A. V. Ivlev, and G. E. Morfill, Phys. Rev. Lett. **108**, 135005 (2012).

[8] V. Nosenko, S. K. Zhdanov, and G. E. Morfill, Phys. Rev. Lett. **99**, 025002 (2007).

[9] H. Thomas and G. Morfill, Nature (London) **379**, 806 (1996).

[10] D. Samsonov, J. Goree, Z. W. Ma, A. Bhattacharjee, H. M. Thomas, and G. E. Morfill, Phys. Rev. Lett. **83**, 3649 (1999).

[11] U. Konopka, G. E. Morfill, and L. Ratke, Phys. Rev. Lett. **84**, 891 (2000).

[12] V. Nosenko, J. Goree, and A. Piel, Phys. Plasmas **13**, 032106 (2006).

[13] S. Nunomura, T. Misawa, N. Ohno, and S. Takamura, Phys. Rev. Lett. **83**, 1970 (1999).

[14] O. S. Vaulina, S. A. Khrapak, A. P. Nefedov, and O. F. Petrov, Phys. Rev. E **60**, 5959 (1999).

[15] A. V. Ivlev, U. Konopka, and G. Morfill, Phys. Rev. E **62**, 2739 (2000).

[16] M. Y. Pustylnik, N. Ohno, S. Takamura, and R. Smirnov, Phys. Rev. E **74**, 046402 (2006).

[17] A. V. Ivlev and G. Morfill, Phys. Rev. E **63**, 016409 (2000).

[18] S. K. Zhdanov, A. V. Ivlev, and G. E. Morfill, Phys. Plasmas **16**, 083706 (2009).

[19] L. Couëdel, V. Nosenko, A. V. Ivlev, S. K. Zhdanov, H. M. Thomas, and G. E. Morfill, Phys. Rev. Lett. **104**, 195001 (2010).

[20] A. V. Ivlev, S. K. Zhdanov, M. Lampe, and G. E. Morfill, Phys. Rev. Lett. **113**, 135002 (2014).

[21] A. V. Ivlev, V. Nosenko, and T. Röcker, Contrib. Plasma Phys. **55**, 35 (2015).

[22] O. Ishihara and S. V. Vladimirov, Phys. Plasmas **4**, 69 (1997).

[23] O. Ishihara, Phys. Plasmas **5**, 357 (1998).

[24] S. V. Vladimirov and A. A. Samarian, Phys. Rev. E **65**, 046416 (2002).

[25] S. V. Vladimirov, S. A. Maiorov, and O. Ishihara, Phys. Plasmas **10**, 3867 (2003).

[26] M. Lampe, G. Joyce, G. Ganguli, and V. Gavrishchaka, Phys. Plasmas **7**, 3851 (2000).

[27] G. A. Hebner, M. E. Riley, and B. M. Marder, Phys. Rev. E **68**, 016403 (2003).

[28] L.-J. Hou, Y.-N. Wang, and Z. L. Mišković, Phys. Rev. E **64**, 046406 (2001).

[29] W. J. Miloch, J. Trulsen, and H. L. Pécseli, Phys. Rev. E **77**, 056408 (2008).

[30] R. Kompaneets, U. Konopka, A. V. Ivlev, V. Tsytovich, and G. Morfill, Phys. Plasmas **14**, 052108 (2007).

[31] R. Kompaneets, S. V. Vladimirov, A. V. Ivlev, and G. Morfill, New J. Phys. **10**, 063018 (2008).

[32] V. A. Schweigert, I. V. Schweigert, A. Melzer, A. Homann, and A. Piel, Phys. Rev. E **54**, 4155 (1996).

[33] A. Melzer, V. A. Schweigert, and A. Piel, Phys. Rev. Lett. **83**, 3194 (1999).

[34] A. V. Ivlev, J. Bartnick, M. Heinen, C.-R. Du, V. Nosenko, and H. Löwen, Phys. Rev. X **5**, 011035 (2015).
[35] L. Couëdel, S. K. Zhdanov, A. V. Ivlev, V. Nosenko, H. M. Thomas, and G. E. Morfill, Phys. Plasmas **18**, 083707 (2011).
[36] R. A. Quinn, C. Cui, J. Goree, J. B. Pieper, H. Thomas, and G. E. Morfill, Phys. Rev. E **53**, R2049 (1996).
[37] S. Zhdanov, R. A. Quinn, D. Samsonov, and G. E. Morfill, New J. Phys. **5**, 74 (2003).
[38] T. E. Sheridan, J. Appl. Phys **98**, 023302 (2005).
[39] T. E. Sheridan, Phys. Plasmas **16**, 083705 (2009).
[40] C. Durniak, D. Samsonov, N. P. Oxtoby, J. P. Ralph, and S. Zhdanov, IEEE Trans. Plasma Sci. **38**, 2412 (2010).
[41] C. A. Knapek, D. Samsonov, S. Zhdanov, U. Konopka, and G. E. Morfill, Phys. Rev. Lett. **98**, 015004 (2007).
[42] J. Schablinski, D. Block, J. Carstensen, F. Greiner, and A. Piel, Phys. Plasmas **21**, 073701 (2014).
[43] L. Couëdel, S. Zhdanov, V. Nosenko, A. V. Ivlev, H. M. Thomas, and G. E. Morfill, Phys. Rev. E **89**, 053108 (2014).
[44] L. D. Landau and E. M. Lifshitz, *Theory of Elasticity* (Pergamon, Oxford, 1986).
[45] T. B. Röcker, S. K. Zhdanov, A. V. Ivlev, M. Lampe, G. Joyce, and G. E. Morfill, Phys. Plasmas **19**, 073708 (2012).
[46] F. M. Peeters and X. Wu, Phys. Rev. A **35**, 3109 (1987).
[47] S. Nunomura, D. Samsonov, and J. Goree, Phys. Rev. Lett. **84**, 5141 (2000).
[48] S. Nunomura, J. Goree, S. Hu, X. Wang, and A. Bhattacharjee, Phys. Rev. E **65**, 066402 (2002).
[49] S. Zhdanov, D. Samsonov, and G. E. Morfill, Phys. Rev. E **66**, 026411 (2002).
[50] T. B. Röcker, A. V. Ivlev, S. K. Zhdanov, and G. E. Morfill, Phys. Rev. E **89**, 013104 (2014).
[51] T. B. Röcker, A. V. Ivlev, R. Kompaneets, and G. E. Morfill, Phys. Plasmas **19**, 033708 (2012).